



ORIGINAL ARTICLE

Plant, Cell & Environment

WILEY

Cell wall modification by the xyloglucan endotransglucosylase/hydrolase XTH19 influences freezing tolerance after cold and sub-zero acclimation

Daisuke Takahashi^{1,2} | Kim L. Johnson^{3,4} | Pengfei Hao^{3,4} | Tan Tuong⁵ | Alexander Erban¹ | Arun Sampathkumar¹ | Antony Bacic^{3,4} | David P. Livingston III⁵ | Joachim Kopka¹ | Takeshi Kuroha^{6,7} | Ryusuke Yokoyama⁶ | Kazuhiko Nishitani^{6,8} | Ellen Zuther¹  | Dirk K. Hincha^{1†} 

¹Max-Planck-Institut für Molekulare Pflanzenphysiologie, Potsdam, Germany

²Graduate School of Science & Engineering, Saitama University, Saitama City, Saitama, Japan

³La Trobe Institute for Agriculture and Food, La Trobe University, Bundoora, Victoria, Australia

⁴Sino-Australian Plant Cell Wall Research Centre, School of Forestry and Biotechnology, Zhejiang A&F University, Hangzhou, China

⁵USDA and Department of Crop Science, North Carolina State University, Raleigh, North Carolina

⁶Graduate School of Life Sciences, Tohoku University, Sendai, Japan

⁷Division of Applied Genetics, Institute of Agrobiological Sciences, National Agriculture and Food Organization (NARO), Tsukuba, Ibaraki, Japan

⁸Faculty of Science, Kanagawa University, Hiratsuka, Japan

Correspondence

Daisuke Takahashi and Ellen Zuther, Max-Planck-Institut für Molekulare Pflanzenphysiologie, Am Mühlenberg 1, D-14476 Potsdam, Germany.
Email: dtakahashi@mail.saitama-u.ac.jp (D.T.) and zuther@mpimp-golm.mpg.de (E.Z.)

Funding information

Alexander von Humboldt-Stiftung, Grant/Award Number: Postdoctoral Fellowship; Deutsche Forschungsgemeinschaft, Grant/Award Number: CRC 973, A3; Japan Society for the Promotion of Science, Grant/Award Number: 27328, 20K15494

Abstract

Freezing triggers extracellular ice formation leading to cell dehydration and deformation during a freeze–thaw cycle. Many plant species increase their freezing tolerance during exposure to low, non-freezing temperatures, a process termed cold acclimation. In addition, exposure to mild freezing temperatures after cold acclimation evokes a further increase in freezing tolerance (sub-zero acclimation). Previous transcriptome and proteome analyses indicate that cell wall remodelling may be particularly important for sub-zero acclimation. In the present study, we used a combination of immunohistochemical, chemical and spectroscopic analyses to characterize the cell walls of *Arabidopsis thaliana* and characterized a mutant in the *XTH19* gene, encoding a xyloglucan endotransglucosylase/hydrolase (XTH). The mutant showed reduced freezing tolerance after both cold and sub-zero acclimation, compared to the Col-0 wild type, which was associated with differences in cell wall composition and structure. Most strikingly, immunohistochemistry in combination with 3D reconstruction of centres of rosette indicated that epitopes of the xyloglucan-specific antibody LM25 were highly abundant in the vasculature of Col-0 plants after sub-zero acclimation but absent in the *XTH19* mutant. Taken together, our data shed new light on the potential roles of cell wall remodelling for the increased freezing tolerance observed after low temperature acclimation.

KEYWORDS

Abiotic stress, *Arabidopsis thaliana*, apoplast, cell wall remodeling, extracellular matrix, xyloglucan, immunohistochemistry

[†] We dedicate this paper to the memory of our colleague Dirk K. Hincha who passed away during the preparation of this manuscript.

1 | INTRODUCTION

Freezing is a severe stress for plants, which is accompanied by a phase transition from liquid water to ice crystals in the tissues. Ice crystallization takes place in the intercellular spaces (Pearce & Willison, 1985). The different chemical potential between intracellular water and extracellular ice leads to the growth of ice crystals at the expense of intracellular water and a concomitant loss of cell volume (Hinch, Heber, & Schmitt, 1990; Steponkus, 1984; Takahashi, Li, Nakayama, Kawamura, & Uemura, 2013). The chemical and mechanical properties of the cell wall will strongly influence cell deformation induced by extracellular freezing and the extent of freeze-thaw damage (Pearce, 1988). In addition, recent work suggests that changes in the properties of the cell wall, elicited by changing environmental conditions, may be sensed by plasma membrane-bound receptor-like kinases that may then in turn elicit signalling cascades that result in changes in wall composition and properties (Gigli-Bisceglia, Engelsdorf, & Hamann, 2020; Johnson, Gidley, Bacic, & Doblin, 2018; Voxeur & Höfte, 2016). In general, the primary plant cell wall is made up of a network of cellulose microfibrils that are embedded in and connected to a matrix of hemicelluloses (such as heteroxylans, heteroglucans, heteromannans) and pectins, consisting of acidic (homogalacturonans, and rhamnogalacturonans I and II) and neutral (arabinans and type 1 (arabino)galactans) components and several (glyco)proteins.

Many plant species increase their freezing tolerance upon exposure to low, non-freezing temperatures (cold acclimation, CA). Previous studies have demonstrated a multitude of changes in gene expression, protein, metabolite and lipid composition during CA (see Guy, Kaplan, Kopka, Selbig, & Hinch, 2008; Thomashow, 2010; Hinch, Espinoza, & Zuther, 2012; Knight & Knight, 2012; Ding, Shi, & Yang, 2019 for comprehensive reviews). Additionally, exposure to mild, non-damaging freezing temperatures subsequent to CA evokes enhanced freezing tolerance and is referred to as sub-zero acclimation (SZA) (Le, Engelsberger, & Hinch, 2008; Le, Pagter, & Hinch, 2015; Livingston, 1996; Livingston & Henson, 1998; Livingston, Van, Premakumar, Tallury, & Herman, 2007; Oliën, 1984; Takahashi et al., 2019; Trunova, 1965).

The freezing tolerance of the *Arabidopsis* accession Columbia-0 (Col-0) is approximately 2–4°C higher after 1–2 weeks of CA at 4°C than in the non-acclimated state (NA) (Hannah et al., 2006; Uemura, Joseph, & Steponkus, 1995; Zuther, Schulz, Childs, & Hinch, 2012). The plants gain a further 3–4°C of freezing tolerance after SZA treatment at –3°C for 3 days (Le et al., 2008; Takahashi et al., 2019). The molecular basis of SZA is not well understood. No significant increases in the cellular content of compatible solutes such as sugars and proline have been observed during SZA (Le et al., 2008) and there is little overlap between changes in gene expression profiles after CA and SZA (Le et al., 2008, 2015). These results indicate that the higher freezing tolerance acquired during SZA is attained by mechanisms different from CA.

Transcriptome analysis of *Arabidopsis* leaves during SZA indicated an over-representation of cell wall-related genes among

significantly up-regulated genes (Le et al., 2015). These included the xyloglucan endotransglucosylases/hydrolases (XTHs) *XTH18* and *XTH19*, which were significantly upregulated at all three timepoints (8 h, 1 day, 3 days) of SZA investigated in this study. This is in accordance with changes in the extracellular proteome of *Arabidopsis* leaves after 3 days of SZA, in particular affecting the abundance of several pectin methylesterases (PMEs), pectin methylesterase inhibitors (PMEIs), and XTHs (Takahashi et al., 2019). In parallel, an increase in total cell wall amount after CA, as well as structural and compositional changes in the cell walls during both CA and SZA was observed (Takahashi et al., 2019). CA-induced increases of cell wall content, thickness and rigidity have also been reported in other plant species (Domon et al., 2013; Griffith, Huner, Espelie, & Kolattukudy, 1985; Kubacka-Zębalska & Kacperska, 1999; Rajashekar & Burke, 1996; Rajashekar & Lafta, 1996; Solecka, Zebrowski, & Kacperska, 2008; Weiser, Wallner, & Waddell, 1990) and may be accompanied by the modification of pectins and hemicelluloses (Kubacka-Zębalska & Kacperska, 1999; Willick, Takahashi, Fowler, Uemura, & Tanino, 2018). In addition to changes in the cell wall itself, compositional changes of apoplastic solutes such as fructans (Livingston & Henson, 1998; Trunova, 1965; Valluru, Lammens, Claupein, & Van den Ende, 2008; Valluru & Van den Ende, 2008) and the accumulation of antifreeze and ice binding proteins (Duman & Olsen, 1993; Griffith & Yaish, 2004) have been described for the apoplast during CA.

There is, however, only limited information available on how changes in cell wall composition and structure influence plant freezing tolerance. Studies of knockout mutants have shown that reduced content of lignin in the secondary cell wall of *Arabidopsis* is associated with increased freezing tolerance after CA (Ji et al., 2015). On the other hand, inactivation of a gene encoding an enzyme catalysing the first step in the conversion of GDP-mannose to GDP-fucose (MUR1; GDP-D-mannose-4,6-dehydratase), the nucleotide sugar donor for the biosynthesis of cell wall fucose-containing polysaccharides, results in lower fucose levels in cell walls, leading to reduced boron-dependent dimerization of pectic domains in rhamnogalacturonan II and reduced leaf freezing tolerance after CA (Panter et al., 2019). Further, overexpression of a PME in *Arabidopsis* results in lower PME activity and reduced freezing tolerance in NA plants (Chen et al., 2018). To the best of our knowledge, no corresponding data on SZA have been published.

In the present study, we focus on xyloglucan, a primary component of hemicellulose of dicots, and the gene *XTH19* encoding a xyloglucan-modifying enzyme. Xyloglucan binds non-covalently to cellulose and forms a xyloglucan-cellulose network (Park & Cosgrove, 2015; Rose, Braam, Fry, & Nishitani, 2002). XTHs are responsible for the cleavage and/or rearrangement of the xyloglucan backbone via endotransglucosylase or endohydrolase activities (Eklöf & Brumer, 2010; Rose et al., 2002). Xyloglucan has been considered as a crucial component of the primary plant cell wall, regulating wall extensibility during growth and development. This hypothesis remains controversial as xyloglucan mutants display only moderate growth defects (Park & Cosgrove, 2015). The *XTH19* gene was identified as SZA-induced in a previous study (Le et al., 2015). In this

context, we evaluate the freezing tolerance of T-DNA insertion mutants of the four closely related genes *XTH17* to *XTH20* under different acclimation conditions and provide detailed analysis of cell wall composition and properties of the *xth19* mutant. Our results suggest that the compositional and architectural/organizational changes of the cell wall observed after both CA and SZA may play a role for increasing freezing tolerance and highlight the functional role of XTH19 via xyloglucan remodelling in these cell wall responses.

2 | MATERIALS AND METHODS

2.1 | Plant cultivation and determination of freezing tolerance

The *Arabidopsis thaliana* ecotype Columbia-0 (Col-0) was used as wild type (WT) in this study. The T-DNA insertion mutants *xth17* (SALK_015077; AT1G65310), *xth18* (SALK_025862C; AT4G30280), *xth19* (SALK_034274; AT4G30290) and *xth20* (SAIL_575_H09; AT5G48070) and the corresponding promoter_{XTH}::GUS expression lines were obtained according to Vissenberg et al. (2005) and Osato, Yokoyama, and Nishitani (2006), and from the Arabidopsis Biological Resource Centre (ABRC). T-DNA insertion in the target genes was confirmed by polymerase chain reaction (PCR) amplification (Figure S1). All primers used in PCR are listed in Table S1.

Plants were grown in soil in a greenhouse at 20°C during the day and 18°C during the night until 35 days after sowing (non-acclimated plants, NA) as described previously (Takahashi et al., 2019). Plants were then transferred into a growth chamber at 4°C with a 16 h photoperiod (90 $\mu\text{mol m}^{-2} \text{s}^{-1}$) for an additional 7 days (cold acclimation, CA). For SZA and extended cold acclimation (CA+), whole rosettes from CA plants were placed in the bottom of 500 mL glass vials containing 20 mL distilled water and immediately placed into a temperature-controlled silicon oil bath (Huber, Offenburg, Germany) at -3°C (SZA) or 4°C (CA+) for 3 days in the dark (Takahashi et al., 2019). During the entire incubation at -3°C, we did not visually observe ice crystallization in the vials. This material was used for subsequent immunohistochemistry and isolation of cell wall material (CWM).

Freezing tolerance of detached leaves was determined as the LT₅₀ using an electrolyte leakage assay (Thalhammer, Hinch, & Zuther, 2014). In this case, detached leaves were incubated in glass tubes, with their petioles placed in distilled water, for SZA and CA+ treatments. For the freezing treatment, ice crystallization was induced at -1°C for NA, CA and CA+, and at -3°C for SZA (Takahashi et al., 2019).

2.2 | Immunohistochemistry

Leaves (leaf number 5 from the youngest fully developed leaf) were cut into strips and put into freshly prepared fixative solution (10 mL 10% paraformaldehyde, 250 μL 25% glutaraldehyde, 2.5 mL 10x PBS,

12.25 mL H₂O). Tissues were immersed under vacuum for 1 h and fixative was discarded. Samples were vacuum infiltrated again for 3 h with fresh fixative. Samples were then washed three times with PBS for 30 min at 4°C. Tissues were dehydrated by sequential immersion in increasing concentrations of ethanol (30%–100%, v/v) at 4°C and then embedded in LR White resin (Electron Microscopy Science, Hatfield, PA) at 4°C by incubation with increasing concentrations of LR white in ethanol. Leaf samples were placed in gelatin capsules filled with LR white and incubated at 60°C for at least 3 days to polymerize the resin. Ultrathin sections at 250 nm were cut with a Leica Ultramicrotome UC6 (Leica Microsystems, Wetzlar, Germany). Sections were incubated for 30 min in blocking buffer containing 3% (w/v) skimmed milk powder in PBS and then rinsed with PBS. Subsequently, the sections were incubated for 2 h in primary antibodies (PlantProbes, Leeds, United Kingdom) diluted 1:10 with PBS. Sections were then rinsed in PBS and subsequently incubated for 1 h in Alexa Fluor 488-tagged secondary antibody (Invitrogen, Waltham, MA) diluted 100x in PBS. Cell walls were stained with 0.1% Calcofluor White in PBS for 2 min. Sample imaging was performed with an epifluorescence microscope (BX-61, Olympus, Tokyo, Japan).

For the investigation of the centre of rosettes in Arabidopsis, WT and *xth19* plants after NA, CA, CA+ and SZA were processed using a microwave-assisted protocol as described by Livingston, Tuong, Haigler, Avci, and Tallury (2009) with some modifications. Tissues were dehydrated in solutions containing a 5% increment of ethanol, from 70% to 100% (v/v) at 32°C and 600 watts for 10 min at each step followed by clearing with xylene. Whole plants including part of the leaf blades, petioles, stem and roots were embedded in paraffin (Paraplast Plus, Ted Pella Inc., Redding, CA) overnight. The embedded samples were sectioned the following day at a thickness of 10 μm using a Leica RM2255 microtome (Leica Biosystems, Wetzlar, Germany). Sections were floated and dried overnight on 1 mm glass slides (Gold Seal Rite-On Frosted Slides, Ted Pella Inc., Redding, CA) using a 0.35% (v/v) Elmer's Carpenter's Wood glue (Elmer's, Westerville, OH). Preliminary testing revealed no effect on fluorescence signal from the dilute glue solution.

To prepare for immunohistochemistry, the sectioned samples were de-paraffinized and rehydrated as described by Crosby et al. (2017). Paraffin-infiltrated tissues were placed in xylene twice for 10 min each. They were then placed in a 1:1 xylene: ethanol solution and a series of graded ethanol: water solutions (from 100%–50% ethanol, in 10% increments) for 5 min each. To insure that all samples were subjected to identical conditions during immuno-histochemistry, eight sections derived from all four treatments of both WT and *xth19* plants were included on the same slide.

Various concentration and incubation times with Toluidine Blue O (Biggs, 1985) were tested to optimize conditions that would minimize auto-fluorescence but not the antibody signal. Optimum parameters were 3 h in 0.5% (w/v) Toluidine Blue O blue at room temperature. Slides were then rinsed three times in phosphate-buffered saline solution containing 0.05% Tween 20 (PBST) and were subsequently incubated for 1 h in a blocking solution of 3% (w/v) bovine serum albumin in PBST. LM25 primary antibody diluted 1:10

in blocking solution was added to cover all sections on a slide. Sections were incubated in the primary antibody solution overnight at room temperature in a sealed container. Slides were then rinsed three times with PBST and incubated for 4 h at room temperature with the fluorescently labelled (Alexa Fluor 488) secondary antibody diluted 1:100 in blocking solution. Slides were then rinsed three times in PBST and subsequently dehydrated through an ethanol series (50%–100%, 10% increments) before they were mounted with Permount (Fisher Scientific, Pittsburgh, PA) and covered with a cover-glass.

Images were captured at an exposure time of 1 s (at F5.6) with a Canon Rebel consumer grade camera mounted on a Nikon Eclipse 50i fluorescence microscope at 200X using a Nikon GFP/F Long Pass filter set with an excitation wavelength of 450–490 nm and a barrier at 500 nm. Images of sections for use in 3D reconstruction were imported into Adobe After Effects (Adobe Systems Inc., San Jose, CA) and processed using a technique described previously (Livingston & Tuong, 2014). Briefly, background colour (black) was digitally removed from each image; images were then manually aligned with each other and separated in z-space. Video S1 is a sequence of all 90 images used in the 3D reconstruction in Video S2. Each image is labelled with the number of the corresponding section to allow easy retrieval so that higher magnification images can be captured. Once images were distributed in z-space, animation parameters were applied to produce the 3D visualization of the antibody signal shown in Video S2.

2.3 | GUS staining

Histochemical analysis to detect GUS reporter enzyme activity was performed as described by Jefferson, Kavanagh, and Bevan (1987) with some modifications (Bolt, Zuther, Zintl, Hinch, & Schmölling, 2017).

2.4 | Isolation and fractionation of CWMs

CWM was extracted from frozen, ground tissue by sequential extraction with 80% (v/v) ethanol, acetone and methanol as described by Takahashi et al. (2019). Starch was removed by α -amylase digestion. Cell wall polysaccharides were precipitated with ethanol at -20°C for 1 h, pellets were washed three times with ethanol and then air-dried to generate the alcohol-insoluble residue (AIR).

Approximately 30 mg of CWM was transferred into a screw-capped microtube for sequential cell wall fractionation as follows: (1) 50 mM 1,2-diaminocyclohexane tetraacetic acid (CDTA, adjusted to pH 6.5 with NaOH), (2) 50 mM Na_2CO_3 (supplemented with 20 mM NaBH_4), (3) 4 M KOH (supplemented with 20 mM NaBH_4). Each extraction was performed at 4°C for 12 h and repeated twice. The final pellets were washed three times with distilled water. Na_2CO_3 and KOH fractions were acidified to pH 5.0 with acetic acid. All four fractions were dialyzed with Spectra/Por dialysis tubes (MWCO: 3.5 kDa, Spectrum Laboratories, Rancho Dominguez, California) for 3 days at 4°C against distilled water, which was exchanged every 12 h. All fractions were dried by lyophilization (Christ, Osterode, Germany).

Around 1 mg of all five fractions (CWM, CDTA, Na_2CO_3 , KOH and insoluble) was transferred into screw-capped microtubes and subjected to further compositional analysis. Three biological replicates of each treatment (NA, CA, SZA and CA+) were prepared for both WT and *xth19*.

2.5 | Alditol acetate-based analysis of cell wall monosaccharides

Neutral non-cellulosic monosaccharide composition of all cell wall fractions was determined by gas chromatography–mass spectrometry (GC–MS). Aliquots (100 μL) of supernatants after TFA hydrolysis as described previously (Takahashi et al., 2019) were dried on a heating block under N_2 gas. Subsequently, monosaccharides were converted to alditol acetates as described (Albersheim, Nevins, English, & Karr, 1967; Neumetzler, 2010). Detection was performed with an Agilent (Waldbronn, Germany) 6890N GC System coupled with ALeco Pegasus III Mass Spectrometer (Leco, Mönchengladbach, Germany). Peaks were annotated by comparison with reference substances. Absolute amounts were determined by comparison with calibration curves obtained from dilution series of reference substances (see Takahashi, Zuther, & Hinch, 2020 for details).

2.6 | Analysis of cell wall polysaccharides

AIR material was prepared as described previously (Albersheim et al., 1967; Neumetzler, 2010) which was adapted from Sims, Munro, Currie, Craik, and Bacic (1996) as well as Kim and Carpita (1992). The acetic/nitric protocol was adapted from Updegraff (1969). Linkage analysis was performed as outlined in Pettolino, Walsh, Fincher, and Bacic (2012).

2.7 | ATR-FTIR spectroscopy

The FTIR spectra were obtained from dry powder of CWM and the different cell wall fractions using a PerkinElmer Spectrum GX (Waltham, MA) infrared spectrometer equipped with a Golden Gate single reflection diamond ATR system (Specac Ltd., Orpington, Kent, United Kingdom) as described in Takahashi et al. (2019).

2.8 | Statistical analysis

All experiments were conducted with at least three biological replicates as detailed in the figure legends.

Statistical significance was determined by Student's *t* test for two-group comparison and Tukey–Kramer test for multiple comparisons at the $p < .05$ level. The data from FTIR analysis were Pareto-scaled for principal component analysis (PCA) using the *prcomp* function in the R software.

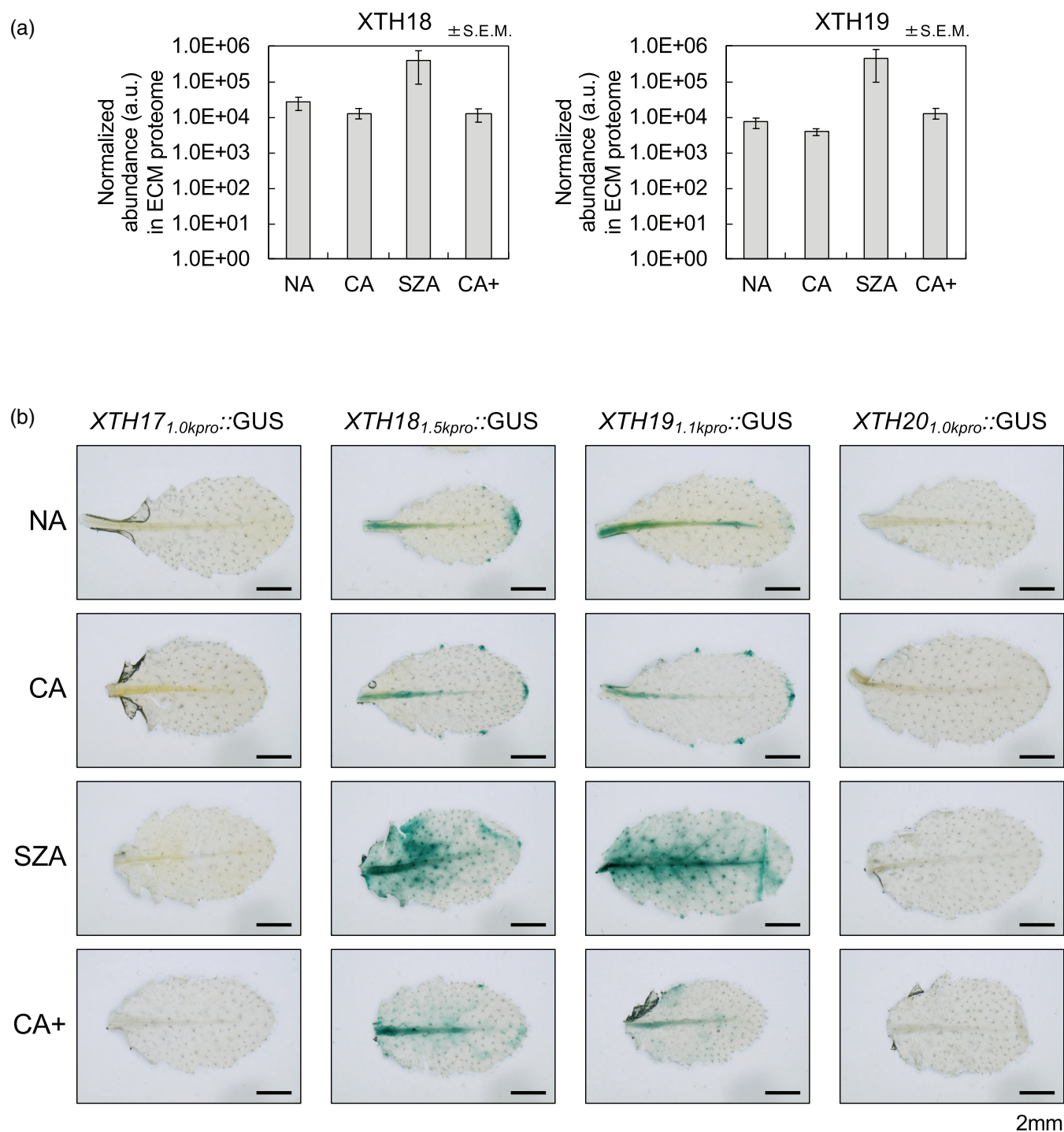


FIGURE 1 Abundance of the XTH19 protein and tissue expression pattern of *XTH17* to *XTH20*. (a) Normalized abundance of the XTH18 and XTH19 protein under non-acclimated (NA) conditions and after 1 week of cold acclimation at 4°C (CA), after subsequent sub-zero acclimation at −3°C for 3 days (SZA) and after prolonged cold acclimation at 4°C for 3 days after CA (CA+). Data were extracted from a proteomic analysis of the extracellular matrix published in Takahashi et al. (2019). Bars represent means of three biological replicates \pm S.E.M. (b) Histochemical analysis of the expression patterns of promoter_{XTH}::GUS constructs for the *XTH17*, *XTH18*, *XTH19* and *XTH20* promoters. The length of the promoter fragments (in kb) is indicated in the figure. Plants were grown at NA condition for 35 days and at CA condition for additional 7 days followed by a SZA or CA+ treatment for 3 days. Fully developed fifth leaves from plants after different treatments were used to visualize promoter activity by GUS staining assay

3 | RESULTS

3.1 | The SZA-responsive protein XTH19 is required for full acclimation during CA and SZA

In all experiments reported in this study, in addition to NA, CA and SZA, an extended cold acclimation treatment of 3 days at 4°C (CA+), as described in our previous study, was applied (Takahashi et al., 2019). Since CA rosettes were detached from soil-grown plants and then incubated at −3°C for 3 days in the dark for the SZA treatment, this could influence the results obtained after SZA. Therefore, CA+ samples were detached and treated in parallel with SZA samples, but at 4°C. The differences of the normalized abundances of XTH18 and XTH19 in the ECM proteome between either CA or CA+, and SZA were not statistically significant, but a trend of accumulation of these proteins was observed (Figure 1a). An additional proteome analysis showed similar results, with statistically significant differences in XTH18 and XTH19 protein abundances between SZA and CA, but no significant differences between SZA and CA+ (Figure S2). A previous transcriptomic study indicated that both the *XTH18* and *XTH19* gene were significantly induced during SZA (Le et al., 2015).

XTH18 and *XTH19* showed similar SZA responses and are members of a small gene family that also includes the phylogenetically closely related genes *XTH17* and *XTH20* (Vissenberg et al., 2005), while *XTH22*, *XTH31* and *XTH33* responded differently to CA and SZA treatments and are phylogenetically more distant to each other. Therefore, in this study, we concentrated on the most promising *XTH* gene subgroup consisting of *XTH17*, *XTH18*, *XTH19* and *XTH20*. Transgenic Arabidopsis plants expressing the β -glucuronidase (*GUS*) gene under the control of approximately 1–1.5 kb of the *XTH17* to *XTH20* promoters (Vissenberg et al., 2005) were exposed to acclimation treatments to determine the expression patterns of

these genes in mature leaves (Figure 1b). While *XTH17* and *XTH20* were only weakly expressed throughout the leaves under all investigated conditions, *XTH18* and *XTH19* were mainly expressed in the leaf veins under NA, CA and CA+ conditions. However, expression increased and spread throughout the leaves during SZA, indicating a potential role of the corresponding proteins in the acclimation process.

To test whether the *XTH17* to *XTH20* genes play a role in plant CA and/or SZA, homozygous T-DNA insertion lines (Osato et al., 2006) (Figure S1) were compared to Col-0 WT plants. Osato et al. (2006) described that the T-DNA insertion mutants of *xth17* (SALK_015077), *xth19* (SALK_034274) and *xth20* (SAIL_575_H09) exhibited altered expression of the target genes. *xth17* showed less than 10%, and *xth19* showed 66% less expression of the respective genes, compared to WT (Osato et al., 2006). On the other hand, the *XTH20* gene showed a four-fold increase in expression in the *xth20* mutant. Expression of the *XTH18* gene in the *xth18* mutant was not reported (Osato et al., 2006).

Freezing tolerance of detached leaves from WT, *xth17*, *xth18*, *xth19* and *xth20* was evaluated using a well-established electrolyte leakage assay (Thalhammer et al., 2014). While *xth20* showed no difference in freezing tolerance compared to WT under any of the acclimation conditions, *xth17* and *xth18* exhibited approximately 1°C lower freezing tolerance (i.e., higher LT₅₀) than WT after CA, but not after CA+ (Figure 2). On the other hand, *xth19* showed significantly less freezing tolerance under all conditions. In particular, the largest difference between WT and *xth19* was observed after SZA (2.44°C). This decrease of freezing tolerance was not due to a general physiological impairment of the plants, as *xth19* exhibited no differences in rosette diameter from WT and had a slightly higher fresh weight (Figure S1c,d). *xth19* had slightly broader leaves than WT, but overall morphology was unaltered (Figure S1e).

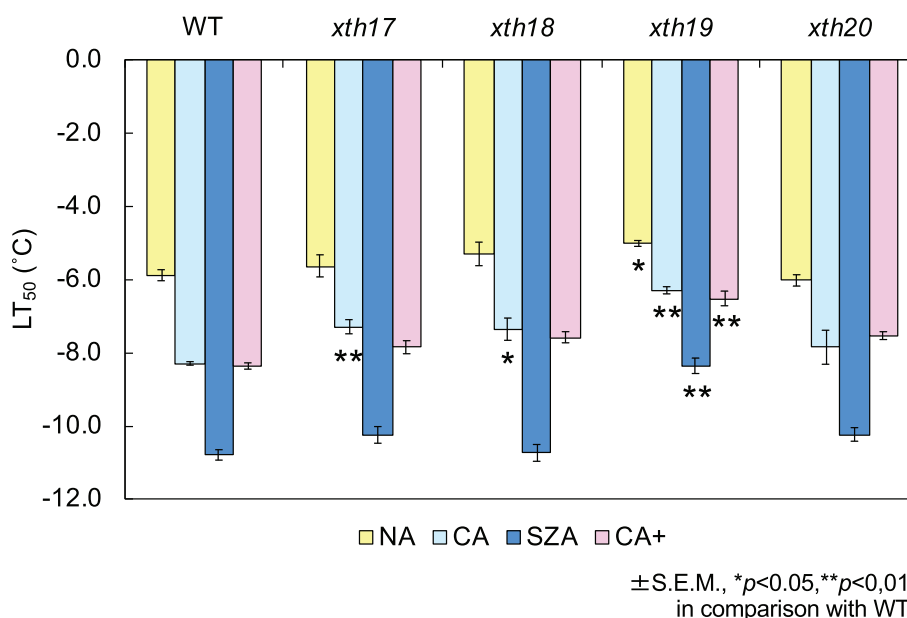


FIGURE 2 Freezing tolerance of *xth* mutants. Influence of T-DNA insertions in the *XTH17*, *XTH18*, *XTH19* and *XTH20* genes on the freezing tolerance of Arabidopsis leaves. Freezing tolerance is expressed as LT₅₀ from electrolyte leakage assays in NA, CA, SZA and CA+ conditions. Error bars indicate ±S.E.M. ($n = 4$) and significant differences between WT and mutants under the same conditions (Student's *t* test) are marked by asterisks

3.2 | XTH19 affects the composition of cell wall polysaccharides

Since XTH19 is an enzyme that remodels the xyloglucan chains, we next investigated the influence of the mutation in XTH19 on cell wall composition (Figure S3). As reported previously (Takahashi et al., 2019), the amount of total CWM was increased during CA, but was not further changed during either SZA or CA+ in WT Col-0. The same pattern was also observed in the *xth19* mutant. Further, a

sequential extraction of the CWM was carried out to separate pectin (1,2-diaminocyclohexane tetraacetic acid (CDTA) and Na_2CO_3 fractions), hemicellulose (KOH fraction) and an insoluble fraction containing mainly cellulose. This analysis revealed no differences in the proportions of these fractions between WT and *xth19*.

Changes in the monosaccharide composition of the non-cellulosic cell wall polysaccharides were analysed by alditol acetate-based GC-MS analysis following TFA hydrolysis (Figure S4 and Table S2). In the WT, Ara and Gal were increased in the unfractionated CWM and in

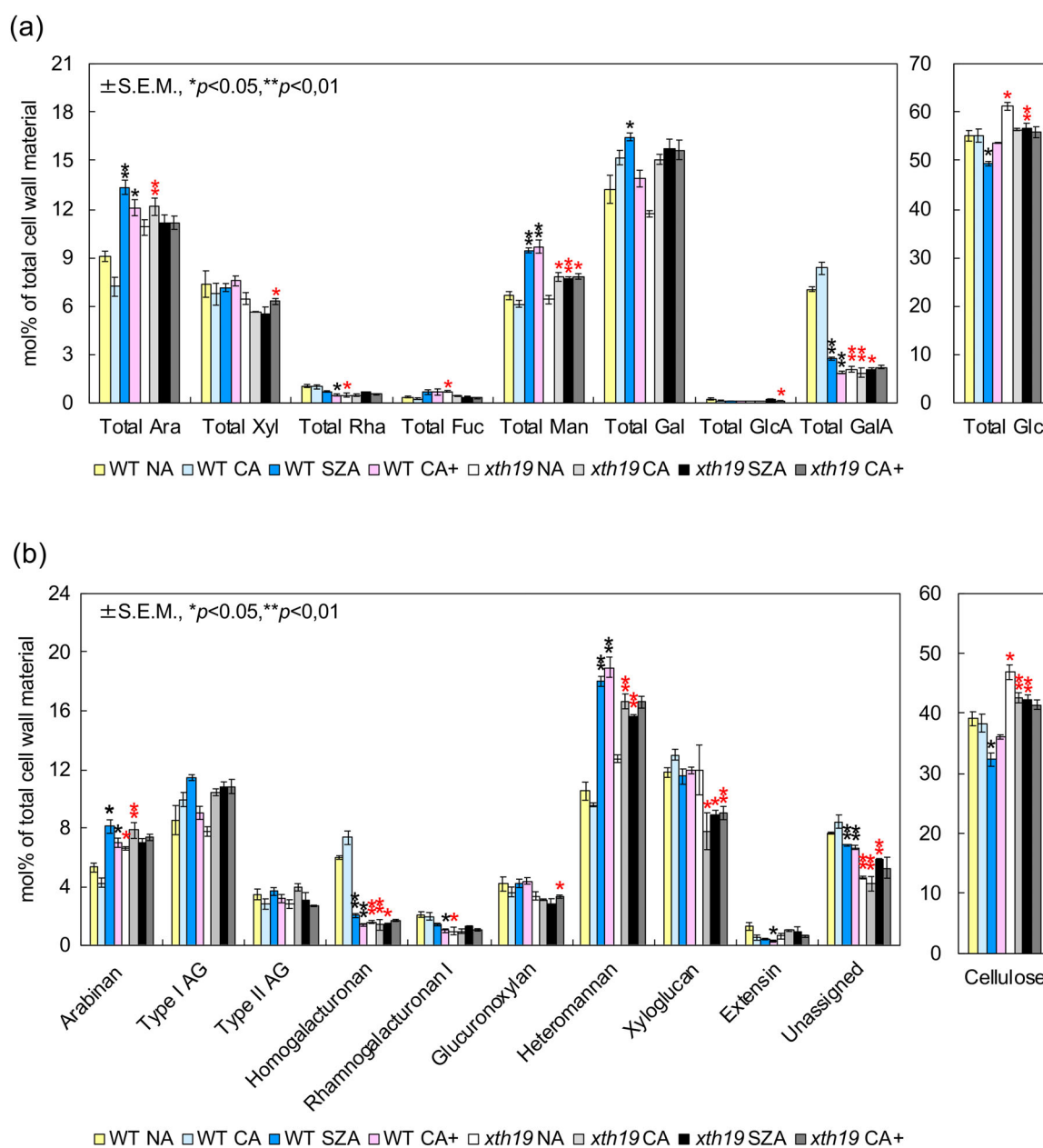


FIGURE 3 Cell wall monosaccharide and polysaccharide composition in WT and *xth19* under different acclimation conditions. The fraction (mol%) of each monosaccharide (a) and polysaccharide (b) composing the total cell wall material are shown. Error bars indicate \pm S.E.M. ($n = 3$). Significant differences (Student's t -test) between NA and the other acclimation conditions in WT are marked with black asterisks. Significant differences between WT and *xth19* under each condition are marked with red asterisks. AG and RG indicate arabinogalactan and rhamnogalacturonan, respectively, while Glc A and Gal A denote glucuronic and galacturonic acid

the CDTA fractions after SZA compared with CA (Figure 4a,b, Takahashi et al., 2019). In the *xth19* mutant, the unfractionated CWM and the pectin-rich Na_2CO_3 fraction contained higher proportions of Xyl than the WT under both CA and SZA conditions (Figure S4a, c). Interestingly, the hemicellulose fraction (Figure S4d) showed no significant differences in monosaccharide composition between WT and *xth19*, indicating that the mutation did not result in overall compositional changes.

Methylation-based linkage analysis of the polysaccharide composition of CWM (Pettolino et al., 2012) provided complementary information about monosaccharide composition (Figure 3a and Table S3) and also allowed us to determine the composition and abundance of the individual wall polysaccharides of the CWM after solvent extraction. In agreement with the alditol acetate-based analysis, we found only minor changes in monosaccharide composition in WT under the different acclimation conditions. It should, however, be noted that the TFA hydrolysates used for alditol acetate-based analysis did not contain Glc derived from crystalline cellulose, making a direct comparison unfeasible. This is particularly relevant for the observed increase in Glc in the *xth19* mutant compared to WT (Figure 3a) that was not observed by alditol acetate-based analysis and corresponds to an increase in cellulose content evident from polysaccharide compositional analysis (Figure 3b and Table S3). We also observed a significant decrease in homogalacturonan (acidic pectin) content in the mutant, in particular under acclimation conditions. This can be related to the decrease in GalA content in the mutant compared to WT. Heteromannan (a hemicellulose) content was strongly increased during both SZA and CA+ in the WT, suggesting that this response is not specifically evoked by SZA, but rather by a prolonged acclimation treatment. On the other hand, in *xth19*, this increase occurred during CA, while it was maintained during SZA and CA+ (Figure 3b).

Since xyloglucan is the substrate of XTH19 enzymatic activity, we have highlighted xyloglucan linkage composition in detail in Figure 4. The total amount of xyloglucan in *xth19* was significantly decreased compared to WT under all acclimation conditions, but not under NA conditions, while the alditol acetate-based method showed different tendencies (Figure S4 and Table S2) probably due to different analytical procedures. The decrease in xyloglucan was reflected in an overall decrease in both 1,4,6-Glcp and 1,4-Glcp, which are major components of the main chain of xyloglucans, in *xth19* under acclimation conditions. The content of Xyl (both 1,2-Xylp and t-Xyl), on the other hand, was unaffected under CA+ and SZA by the *xth19* mutation, although Xyl is also a major component of xyloglucan. On the other hand, *xth19* had higher 1,2-Xylp and lower t-Xyl content during NA and CA. These results indicate that the mutation in XTH19 induced only minor changes in unfractionated CWM composition, most prominently the reduction in xyloglucan content from about 12% to about 9% of CWM and differences in xyloglucan structure.

3.3 | XTH19 affects structural properties of cell walls under acclimation conditions

The small compositional differences between cell walls of WT and *xth19* plants could give rise to structural and architectural changes, such as differences in non-covalent interactions between different polysaccharides that may influence mechanical and rheological properties of cell walls, thus linking composition to freezing tolerance. To assess structural and architectural properties of the cell walls and their component fractions under different acclimation conditions, we performed ATR-FTIR spectroscopy, which is sensitive to compositional and structural differences. We analysed the spectra by PCA (Figure 5). In CWM isolated from either WT or *xth19*, all acclimated samples were separated from NA samples along PC1, which explained about 46% and 54% of the total variance in

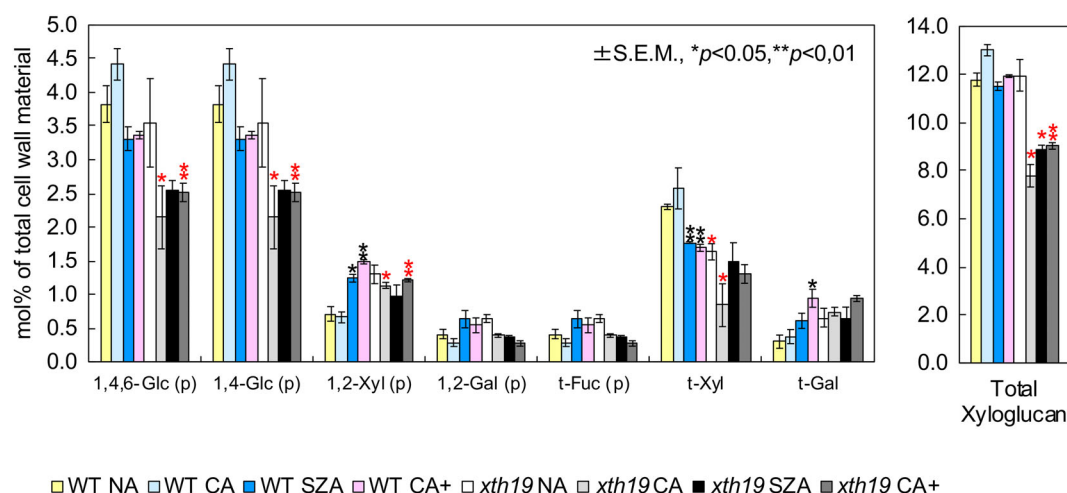


FIGURE 4 Linkage analysis of xyloglucan components in WT and *xth19*. The fraction of total xyloglucan (see Figure 3b) and of each xyloglucan component was calculated relative to the total cell wall material. Error bars indicate \pm S.E.M. ($n = 3$). Significant differences between NA and the other acclimation conditions in WT are marked with black asterisks. Significant differences between WT and *xth19* under each condition are marked with red asterisks. t and (p) indicate terminal and pyranose, respectively

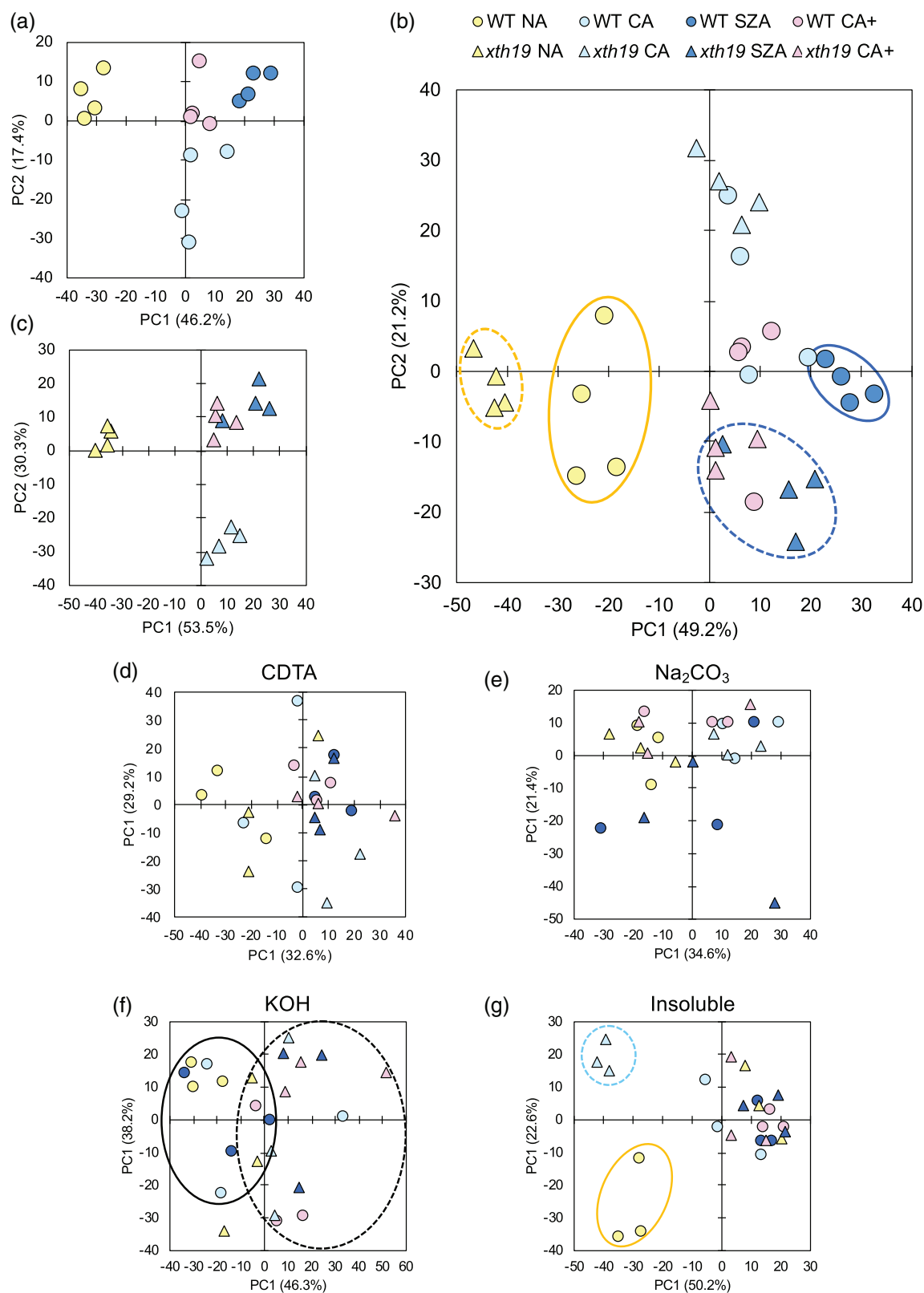


FIGURE 5 Principal component analysis (PCA) of FTIR spectra obtained from cell wall fractions isolated from leaves of WT and *xth19* plants under NA, CA, SZA and CA+ conditions. Dry total cell wall material and the four different cell wall fractions (compare Figure S4) were subjected to ATR-FTIR spectroscopy. Score plots from PCA analysis of the spectra are shown for principal component (PC) 1 and PC2. The fraction of the total variance explained by each PC is indicated in parenthesis. PCA for total cell wall material prepared from WT (a) and *xth19* (b) were performed separately and in addition on the complete dataset (c). Combined PCA was further performed with the FTIR spectra of the CDTA (d), Na_2CO_3 (e), KOH (f) and insoluble (g) fractions

the data from WT and mutant, respectively (Figure 5a,b). The samples from acclimated plants (CA and CA+) were separated along PC2, explaining about 17% (WT) and 30% (*xth19*) of the total variance. The SZA samples from WT plants were separated from the CA+ samples along PC1, while this separation was less pronounced in *xth19*.

When the spectra obtained from WT and *xth19* samples were subjected to a joint PCA, a similar separation according to the different treatments was observed (Figure 5c). In addition, CWM samples from NA and SZA-treated plants showed a clear separation between WT and mutant plants. When the four cell wall fractions were separately subjected to ATR-FTIR analysis and the spectra submitted to PCA, no differences between WT and *xth19* were apparent in the pectin-enriched CDTA and Na_2CO_3 fractions (Figures 4e and 5d). Score plots of spectra obtained from hemicellulose-rich KOH-soluble cell wall fractions, however, showed a clear separation between the genotypes by PC1 (Figure 5f), indicating an influence of XTH19 activity on the structure of these polysaccharides. The insoluble

fractions indicated no clear differences between WT and mutant, however, WT NA and *xth19* CA samples formed two separate clusters (Figure 5g).

3.4 | XTH19 is involved in the distribution of xyloglucan epitopes detected by the LM15 and LM25 antibodies

Since the results described above clearly indicate both compositional and structural differences in the hemicellulose fraction of the cell walls between WT and *xth19* plants under acclimation conditions, we conducted an immune-histochemical analysis of specific hemicellulose epitopes. We used the LM15 (Marcus et al., 2008) and LM25 (Pedersen et al., 2012) antibodies, which respectively recognize XXXG (X = xylose bound to G unit; G = glucose) and XXXG/XXLG/XLLG (L = galactose bound to X unit) structural motifs in xyloglucan.

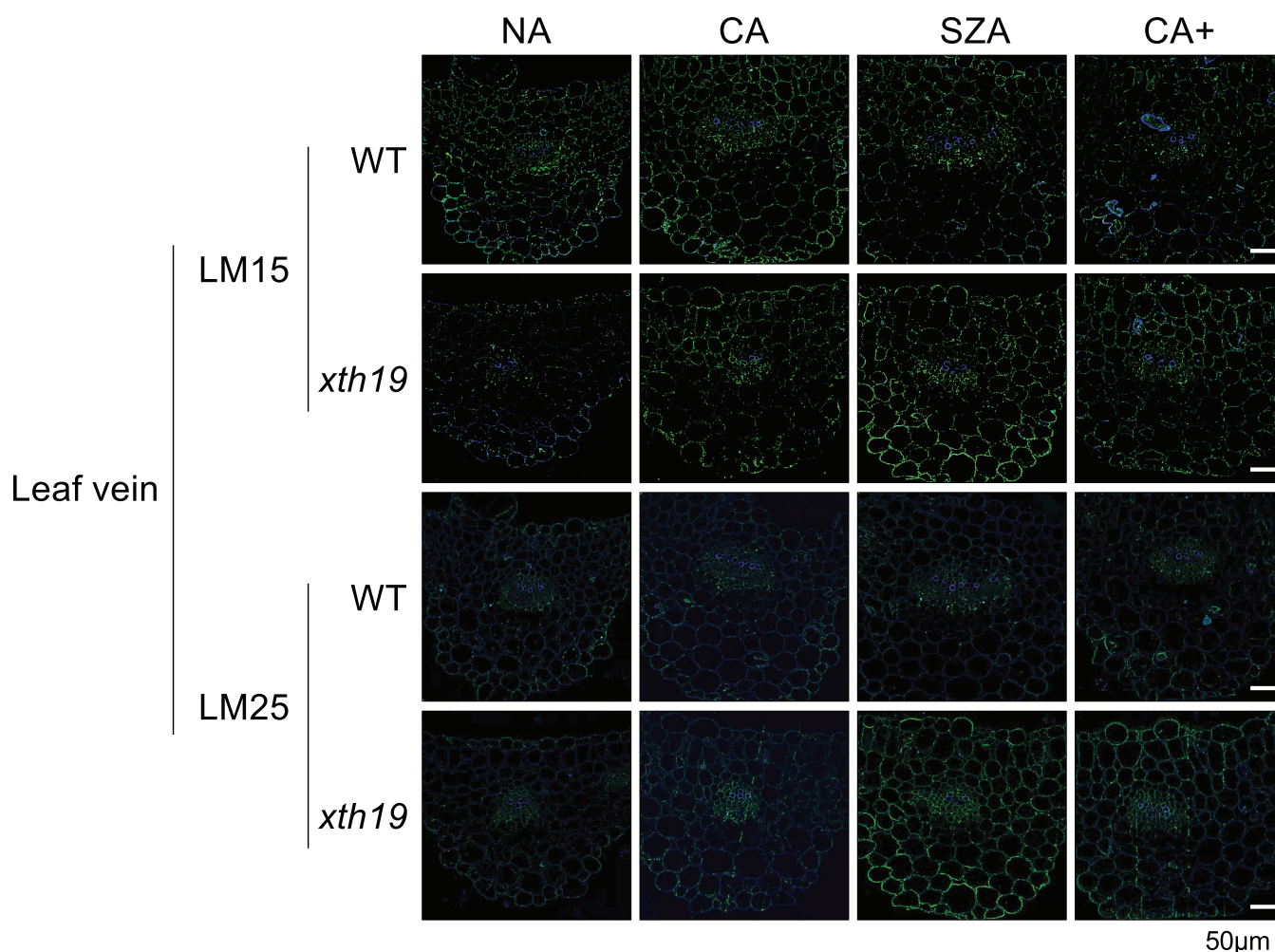


FIGURE 6 Immunohistochemical staining of xyloglucan recognized by the LM15 and LM25 antibodies in leaf vein tissue. Transverse sections of leaf vein tissues were prepared from leaves of WT and *xth19* plants after different acclimation treatments. Plants were grown at NA condition for 35 days and at CA condition for additional 7 days followed by a SZA or CA+ treatment for 3 days. Sections were subjected to immunofluorescence detection of xyloglucan epitopes recognized by the LM15 and LM25 antibodies. Bound antibodies were visualized by a secondary antibody coupled to the Alexa Fluor 488 dye and are indicated in green. Cell walls were highlighted in blue by Calcofluor White. Scale bars indicate 50 μm . Magnification was the same in all panels. Corresponding images of leaf mesophyll tissues are shown in Figure S5

Immunofluorescence images of transverse sections of leaf vein tissues are shown in Figure 6. In WT, patterns of LM15 and LM25 signals were very similar among all acclimation conditions. In contrast, both

LM15 and LM25 signals were strongly increased in *xth19* specifically after SZA. The same patterns were observed in leaf mesophyll tissues (Figure S5).

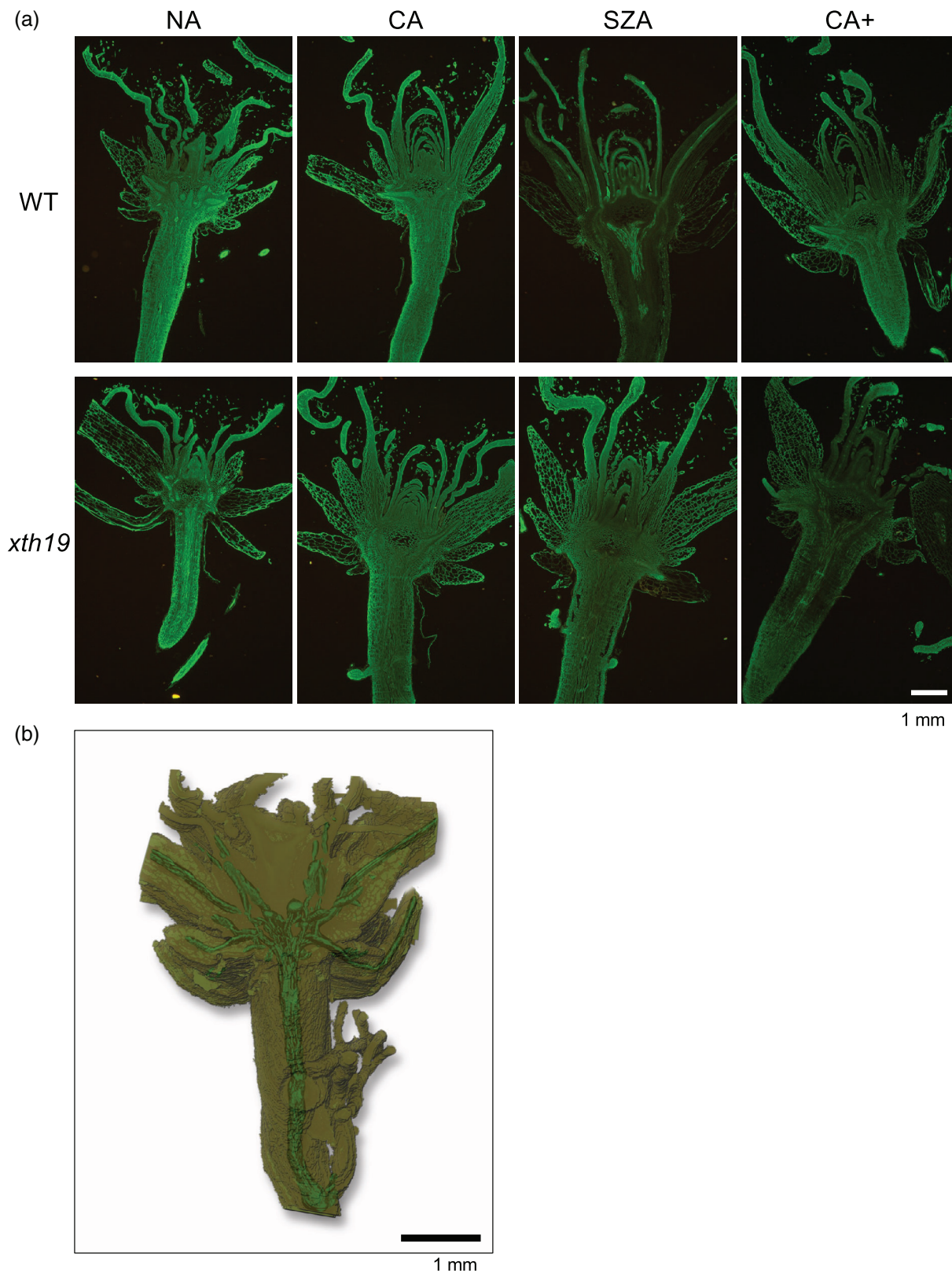


FIGURE 7 Legend on next page.

In addition to fully developed leaves, also centres of rosettes were examined using the LM25 antibody. It has been shown that ice propagation within plants is at least partially controlled by cell wall characteristics in the tissue connecting roots and shoots, such as the crown tissue in monocots (Livingston et al., 2013; Willick et al., 2018) and central parts of *Arabidopsis* rosettes including younger leaves and hypocotyls are crucial for the survival of plants after freeze–thaw damage (Takagi et al., 2003). This ice propagation is one of the determinants of plant freezing tolerance (Livingston et al., 2013; Livingston et al., 2018b). LM25 immunofluorescence signals were ubiquitously distributed in centres of the WT rosette under all conditions except for SZA (Figure 7a), where labelling was largely limited to the central, vascular part of the tissue. On the other hand, the LM25 immunofluorescence in the tissues of *xth19* after SZA was ubiquitous, and not clearly different from the pattern observed under all other conditions, except CA⁺ (Figure 7a). After SZA, weak autofluorescence was observed in young leaves, but not in the vasculature, while under all other conditions no autofluorescence was detectable (Figure S6). To gain deeper insight into the spatial distribution of LM25 epitopes in the centres of rosettes, fluorescence images were obtained from 90 sequential longitudinal sections of a tissue from a WT plant exposed to SZA (Video S1). The images were then used to reconstruct a 3D image (Figure 7b and Video S2). The localization of the immunofluorescence supports our conclusion that under SZA XXXG/XXLG/XLLG epitopes are predominantly detectable in the vasculature of the WT tissues.

4 | DISCUSSION

4.1 | T-DNA insertion in *XTH19* affects freezing tolerance

Among the four investigated *XTH* genes (*XTH17*–*XTH20*) only *XTH19* was induced by 24 h of CA treatment (Tenhaken, 2015). However, after 3 days of CA, *XTH17* was significantly downregulated and *XTH20* upregulated, while *XTH18* and *XTH19* no longer showed significant differences in expression compared to NA (Zuther et al., 2019). After 3 days of SZA after CA, only *XTH18* and *XTH19* were significantly upregulated compared to CA (Le et al., 2015). Based on published (Takahashi et al., 2019) and newly obtained apoplast proteome data, the amounts of *XTH18* and *XTH19* tended to increase during SZA (Figures 1a and S1). Among other members of the XTH

protein family, *XTH22*, *XTH31* and *XTH33* were also identified as significantly (CA-(*XTH22*) or SZA-(*XTH31* and *XTH33*)) induced proteins in the extracellular matrix (ECM) proteome of the *Arabidopsis* accessions Col-0 and N14 (Takahashi et al., 2019).

Likewise, promoter::GUS assays showed increased expression of *XTH18* and *XTH19* during SZA, but not after 7 days of CA, in agreement with the transcript analysis after 3 days (Zuther et al., 2019). However, only *xth19* showed reduced freezing tolerance under these conditions. The *xth19* mutant has a T-DNA insertion at the end of the 3' UTR and has already been used in previous studies (Osato et al., 2006; Wilson et al., 2015). Expression of *XTH19* is not strongly repressed in this mutant (Osato et al., 2006) and the mutant did not show morphological or developmental differences to the WT in either roots or leaves. This has also been observed in another mutant allele (Osato et al., 2006; Pitaksaringkarn et al., 2014). It has been speculated that insertion of the T-DNA in the 3' UTR may stabilize the mRNA and therefore *xth19* may behave like an overexpression line (Wilson et al., 2015). However, *XTH19* overexpression results in faster hypocotyl elongation, a thicker hypocotyl, a >65% increase in wall material and different cell wall biomechanics (Miedes et al., 2013). Since we did not observe corresponding phenotypes in *xth19*, we find it unlikely that this mutation leads to overexpression. Unfortunately, we were not able to detect unique peptides of *XTH19* in either WT or mutant plants in the present study, as the amino acid sequences of *XTH19* and *XTH18* proteins that are encoded by a tandem repeat gene pair are very similar (92%).

4.2 | Potential role of *XTH19* in xyloglucan remodelling

Xyloglucan endotransglucosylases/hydrolases (XTHs) play a role in the remodelling of cell wall hemicellulose by either hydrolysing or remodelling xyloglucans (Rose et al., 2002). XTH enzymes have two possible activities, acting as endotransglucosylases (XET) and xyloglucan endohydrolases (XEH) (Eklöf & Brumer, 2010; Rose et al., 2002). XEH activity only catalyses xyloglucan degradation, while XET can play roles in both integration of newly synthesized xyloglucan into cell wall polysaccharides and suppression of xyloglucan accumulation (Herbers, Lorences, Barrachina, & Sonnewald, 2001; Miedes, Herbers, Sonnewald, & Lorences, 2010; Rose et al., 2002; Zhu et al., 2012). *XTH19* only exhibits XET activity (Maris et al., 2011). Significantly, it is cold adapted and maintains 70% of its maximal activity

FIGURE 7 Immunohistochemical staining of xyloglucan recognized by the LM25 antibody in centres of *Arabidopsis* rosettes. Longitudinal sections prepared from centres of WT and *xth19* rosettes, including shoot apical meristems, were subjected to immunofluorescence detection using the LM25 antibody (compare Figure 6). Plants were grown at NA condition for 35 days and at CA condition for additional 7 days followed by a SZA or CA⁺ treatment for 3 days. The xyloglucan epitopes are indicated as green fluorescent color. (a) Images of immunofluorescence of longitudinal sections of tissues from WT and *xth19* under the different acclimation conditions. Scale bars indicate 1 mm. (b) Internal LM25 epitope distribution shown as a 3D image reconstructed from 90 longitudinal sections of a WT tissue from a plant exposed to sub-zero acclimation conditions (SZA). Corresponding autofluorescence images of WT and *xth19* are shown in Figure S6. 3D images from different angles can be found in Video S1 and all sequential images constituting the 3D image are shown in Video S2

at 4°C, which is the highest activity at this temperature among the investigated enzymes (XTH12, XTH13, XTH17, XTH18 and XTH19) (Maris et al., 2011). This makes it suitable for cell wall remodelling at low temperatures. Both, our data on cell wall composition and the ATR-FTIR data from WT and *xth19* cell walls imply that there is a potential role of XTH19, in particular during SZA leading to acquired freezing tolerance in plants.

4.3 | Structural and compositional changes of xyloglucan during acquisition of freezing tolerance

In WT leaves, immuno-histochemical analysis using the xyloglucan epitope-specific antibodies LM15 and LM25 (Pedersen et al., 2012) revealed only subtle changes during CA and SZA. In agreement with this finding, the amount of xyloglucan was not significantly changed in WT leaves under any acclimation condition. The minor changes in the distribution of LM15 and LM25 epitopes after CA and SZA may be masked by other cell wall polysaccharides such as the acidic pectic homogalacturonan (HG) (Marcus et al., 2008). The amount of HG was significantly lower after SZA and CA+ compared to NA and CA, which may have led to structural rearrangements in the interactions of xyloglucan and HG, resulting in the subtle changes in both LM15 and LM25 epitopes. Heteromannan may also have masking effects like HG as one of the major hemicellulosic polysaccharides, similar to xyloglucan.

Altered xyloglucan deposition as revealed by the LM15 and LM25 antibodies in *xth19* leaves compared to WT were only observed after SZA. Although after CA treatment no corresponding differences between the genotypes were observed, ATR-FTIR analysis showed differences in the hemicellulose-rich KOH fractions between WT and *xth19*. In addition, freezing tolerance was significantly decreased in *xth19* under both CA and SZA. Compositional analysis of cell wall polysaccharides supported these results, as both the amount of total xyloglucan and of its major backbone residues (1,4,6-Glcp and 1,4-Glcp) were lower in *xth19* after both CA and SZA treatments. Interestingly, the effect of the *xth19* mutation on other major components of xyloglucan such as 1,2-Xylp and t-Xyl was different from that on Glc residues, suggesting that both, backbone and side chains of xyloglucans were affected by the mutation. Glc residues of the xyloglucan backbone are partly substituted by O-acetylation on Glc residue that are not xylosylated (Pauly & Keegstra, 2016). The O-acetylation status of the β -1,4-linked glucan backbone in xyloglucan may change during CA and SZA in *xth19* leading to reduced proportions of 1,4,6-Glcp and 1,4-Glcp without changes of other xyloglucan components; these residues are not identified during the base-catalysed methylation reaction for linkage analyses as this removes the O-acetyl residues. These changes can also be associated with the motif frequency in the xyloglucan sequence, which may influence recognition by LM15 and LM25 antibodies. Opposite tendencies of linkage analysis and immunohistochemical results during CA and SZA in the *xth19* mutant may be due to O-acetylation status of xyloglucan and/or masking effect of HG described above. Taken together, these

results suggest that structural and compositional properties of xyloglucan were one of the reasons for the reduced freezing tolerance in the mutant.

On the other hand, microscopic results did not show any marked difference between WT and the mutant during NA and CA. However, freezing tolerance was decreased by the mutation in *XTH19* in these conditions. Other cell wall components exhibited differences between WT and *xth19* under NA and CA, such as arabinan, HG and cellulose. These results suggest that altered xyloglucan modifications and/or interactions between cell wall components due to loss of XTH19 activity might have indirect effects on other cell wall components that contribute to differences in freezing tolerance. Furthermore, a previous study demonstrated that mutation of *XTH21* in *Arabidopsis* leads to decreased average molecular weight of xyloglucan and reduced cellulose content (Liu, Lu, Zhang, Liu, & Lu, 2007). The mutants of *XTH21* and *HAP5A*, an upstream regulator of *XTH21*, display decreased basal freezing tolerance (Shi et al., 2014). Therefore, not only the amount of xyloglucan, but also the length of main and/or side of xyloglucan can influence the properties of a variety of cell wall components and associated changes in biomechanics and architecture might have certain effects on the basal and/or acquired freezing tolerance. In agreement with this conclusion, a mutant lacking xyloglucan (*xxt1/xxt2*) in *Arabidopsis* shows altered cell wall mechanical properties (Cavalier et al., 2008; Park & Cosgrove, 2012), including higher plastic and elastic deformability. Similarly, research using cellulose and cellulose/xyloglucan composites suggests that xyloglucan cross-links between cellulose microfibrils increase the stiffness of the cellulose matrix (Bonilla, Lopez-Sanchez, Gidley, & Stokes, 2016). Treatment of such cellulose/xyloglucan composites with a recombinant XET enzyme leads to increases in deformability due to architectural rearrangements without a reduction in xyloglucan content (Chanliaud, De Silva, Strongitharm, Jeronimidis, & Gidley, 2004). Interestingly, Zhang, Tang, Vavylonis, and Cosgrove (2019) reported that cell wall properties such as stiffness, elastic and plastic deformability can be altered independently of each other, potentially giving plants the ability to fine-tune the properties of their walls according to different environmental conditions. It has been hypothesized that a potential role of XET enzymes could be to facilitate shape changes in cells without loss of mechanical strength (Chanliaud et al., 2004). We would like to extend this hypothesis to suggest that the ability to reversibly change shape during the dehydration-rehydration cycle that invariably occurs during a freeze-thaw cycle is important for cell wall behaviour during freeze-stress and is one of the factors that ultimately determine plant freezing tolerance.

In addition, changes of primary cell wall composition and properties, particularly changes in pectin, are considered to be involved in the regulation of ice propagation during freezing (Kubacka-Zębalska & Kacperska, 1999; Rajashekar & Lafta, 1996; Solecka et al., 2008; Stefanowska, Kuraś, Kubacka-Zębalska, & Kacperska, 1999; Willick et al., 2018), while changes in xyloglucan have not been implicated before. Studies using infrared video thermography showed that ice crystal formation proceeds from roots to shoots along the xylem vessels (Hacker & Neuner, 2007; Livingston, Tuong, Hoffman, &

Fernandez, 2018a; Livingston, Tuong, Murphy, et al., 2018b; Neuner, Xu, & Hacker, 2010; Wisniewski, Lindow, & Ashworth, 1997). The most striking result of our immuno-histochemical analysis is the finding that in the centre of WT rosettes the LM25 epitopes are concentrated in the vasculature after SZA, while they remain diffusely localized in the *xth19* mutant. However, it should be noted that biochemical analyses of cell wall components reflect the amount of xyloglucan as a total of the cell wall fraction and immunohistochemistry results can be affected by masking of epitopes by other cell wall polysaccharides such as pectin (Marcus et al., 2008). Therefore, interactions between xyloglucan and other cell wall polymers, regulated by XTH19, might be one of the factors for acquisition of plant freezing tolerance during acclimation periods. Detailed observations of freezing tolerance and ice propagation behaviour in soil grown plants will be needed to ascertain the role of XTH19 in regulating ice crystal propagation after SZA and its role in freezing tolerance.

ACKNOWLEDGMENTS

We thank Anja Fröhlich and Ines Fehrle (Max-Planck-Institut für Molekulare Pflanzenphysiologie) for helping with the microscopy and GC-MS experiments. This study was in part supported by a Grant-in-Aid for Scientific Research from the Japan Society for the Promotion of Science (#27328 and #20K15494), Postdoctoral Fellowship from the Alexander-von-Humboldt Foundation (to DT) and the German Science Foundation (DFG) through Project A3 of the Collaborative Research Centre CRC973 (to D.K.H.). Open access funding enabled and organized by Projekt DEAL.

CONFLICTS OF INTEREST

The authors declare no conflict of interest. The funders had no role in the design of the study; in the collection, analyses or interpretation of data; in the writing of the manuscript or in the decision to publish the results.

ORCID

Ellen Zuther  <https://orcid.org/0000-0002-7446-0515>

Dirk K. Hincha  <https://orcid.org/0000-0001-6887-4933>

REFERENCES

- Albersheim, P., Nevins, D. J., English, P. D., & Karr, A. (1967). A method for the analysis of sugars in plant cell-wall polysaccharides by gas-liquid chromatography. *Carbohydrate Research*, 5(3), 340–345.
- Biggs, A. R. (1985). Detection of impervious tissue in tree bark with selective histochemistry and fluorescence microscopy. *Stain Technology*, 60(5), 299–304.
- Bolt, S., Zuther, E., Zintl, S., Hincha, D. K., & Schmölling, T. (2017). *ERF105* is a transcription factor gene of *Arabidopsis thaliana* required for freezing tolerance and cold acclimation. *Plant, Cell & Environment*, 40(1), 108–120.
- Bonilla, M. R., Lopez-Sanchez, P., Gidley, M. J., & Stokes, J. R. (2016). Micromechanical model of biphasic biomaterials with internal adhesion: Application to nanocellulose hydrogel composites. *Acta Biomaterialia*, 29, 149–160.
- Cavalier, D. M., Lerouxel, O., Neumetzler, L., Yamauchi, K., Reinecke, A., Freshour, G., ... Keegstra, K. (2008). Disrupting two *Arabidopsis thaliana* xylosyltransferase genes results in plants deficient in xyloglucan, a major primary cell wall component. *Plant Cell*, 20(6), 1519–1537.
- Chanliaud, E., De Silva, J., Strongitharm, B., Jeronimidis, G., & Gidley, M. J. (2004). Mechanical effects of plant cell wall enzymes on cellulose/xyloglucan composites. *Plant Journal*, 38(1), 27–37.
- Chen, J., Chen, X., Zhang, Q., Zhang, Y., Ou, X., An, L., ... Zhao, Z. (2018). A cold-induced pectin methyl-esterase inhibitor gene contributes negatively to freezing tolerance but positively to salt tolerance in *Arabidopsis*. *Journal of Plant Physiology*, 222, 67–78.
- Crosby, K., Simendinger, J., Grange, C., Ferrante, M., Bernier, T., & Standen, C. (2014). Immunohistochemistry protocol for paraffin-embedded tissue sections advertisement. *Cell Signal. Technol*, 86, e50641–e50646. Retrieved from <https://www.jove.com/t/5064/immunohistochemistry-protocol-for-paraffin-embedded-tissue-sections>
- Ding, Y., Shi, Y., & Yang, S. (2019). Advances and challenges in uncovering cold tolerance regulatory mechanisms in plants. *New Phytologist*, 222(4), 1690–1704.
- Domon, J.-M., Baldwin, L., Acket, S., Caudeville, E., Arnoult, S., Zub, H., ... Rayon, C. (2013). Cell wall compositional modifications of *Miscanthus* ecotypes in response to cold acclimation. *Phytochemistry*, 85, 51–61.
- Duman, J. G., & Olsen, T. M. (1993). Thermal hysteresis protein activity in bacteria, fungi, and phylogenetically diverse plants. *Cryobiology*, 30(3), 322–328.
- Eklöf, J. M., & Brumer, H. (2010). The XTH gene family: An update on enzyme structure, function, and phylogeny in xyloglucan remodeling. *Plant Physiology*, 153(2), 456–466.
- Gigli-Bisseggia, N., Engelsdorf, T., & Hamann, T. (2020). Plant cell wall integrity maintenance in model plants and crop species-relevant cell wall components and underlying guiding principles. *Cellular and Molecular Life Sciences*, 77, 2049–2077.
- Griffith, M., Huner, N. P. A., Espelie, K. E., & Kolattukudy, P. E. (1985). Lipid polymers accumulate in the epidermis and mestome sheath cell walls during low temperature development of winter rye leaves. *Protoplasma*, 125(1–2), 53–64.
- Griffith, M., & Yaish, M. W. F. (2004). Antifreeze proteins in overwintering plants: A tale of two activities. *Trends in Plant Science*, 9(8), 399–405.
- Guy, C., Kaplan, F., Kopka, J., Selbig, J., & Hincha, D. K. (2008). Metabolomics of temperature stress. *Physiologia Plantarum*, 132(2), 220–235.
- Hacker, J., & Neuner, G. (2007). Ice propagation in plants visualized at the tissue level by infrared differential thermal analysis (IDTA). *Tree Physiology*, 27(12), 1661–1670.
- Hannah, M. A., Wiese, D., Freund, S., Fiehn, O., Heyer, A. G., & Hincha, D. K. (2006). Natural genetic variation of freezing tolerance in *Arabidopsis*. *Plant Physiology*, 142(1), 98–112.
- Herbers, K., Lorences, E. P., Barrachina, C., & Sonnewald, U. (2001). Functional characterisation of *Nicotiana tabacum* xyloglucan endo-transglucosylase (Nt XET-1): Generation of transgenic tobacco plants and changes in cell wall xyloglucan. *Planta*, 212(2), 279–287.
- Hincha, D. K., Espinoza, C., & Zuther, E. (2012). Transcriptomic and metabolomic approaches to the analysis of plant freezing tolerance and cold acclimation. In N. Tuteja, S. S. Gill, A. F. Tiburcio, & R. Tuteja (Eds.), *Improving crop resistance to abiotic stress* (pp. 255–287). Weinheim, Germany: Wiley-VCH Verlag GmbH & Co. KGaA.
- Hincha, D. K., Heber, U., & Schmitt, J. M. (1990). Proteins from frost-hardy leaves protect thylakoids against mechanical freeze-thaw damage in vitro. *Planta*, 180(3), 416–419.
- Jefferson, R. A., Kavanagh, T. A., & Bevan, M. W. (1987). GUS fusions: Beta-glucuronidase as a sensitive and versatile gene fusion marker in higher plants. *EMBO Journal*, 6(13), 3901–3907.
- Ji, H., Wang, Y., Cloix, C., Li, K., Jenkins, G. I., Wang, S., ... Li, X. (2015). The *Arabidopsis* RCC1 family protein TCF1 regulates freezing tolerance and cold acclimation through modulating lignin biosynthesis. *PLoS Genetics*, 11(9), e1005471.

- Johnson, K. L., Gidley, M. J., Bacic, A., & Doblin, M. S. (2018). Cell wall bio-mechanics: A tractable challenge in manipulating plant cell walls 'fit for purpose'. *Current Opinion in Biotechnology*, 49, 163–171.
- Kim, J. B., & Carpita, N. C. (1992). Changes in esterification of the uronic acid groups of cell wall polysaccharides during elongation of maize coleoptiles. *Plant Physiology*, 98(2), 646–653.
- Knight, M. R., & Knight, H. (2012). Low-temperature perception leading to gene expression and cold tolerance in higher plants. *New Phytologist*, 195(4), 737–751.
- Kubacka-Zębalska, M., & Kacperska, A. (1999). Low temperature-induced modifications of cell wall content and polysaccharide composition in leaves of winter oilseed rape (*Brassica napus* L. var. *Oleifera* L.). *Plant Science*, 148(1), 59–67.
- Le, M. Q., Engelsberger, W. R., & Hinch, D. K. (2008). Natural genetic variation in acclimation capacity at sub-zero temperatures after cold acclimation at 4°C in different *Arabidopsis thaliana* accessions. *Cryobiology*, 57(2), 104–112.
- Le, M. Q., Pagter, M., & Hinch, D. K. (2015). Global changes in gene expression, assayed by microarray hybridization and quantitative RT-PCR, during acclimation of three *Arabidopsis thaliana* accessions to sub-zero temperatures after cold acclimation. *Plant Molecular Biology*, 87, 1–15.
- Liu, Y.-B., Lu, S.-M., Zhang, J.-F., Liu, S., & Lu, Y.-T. (2007). A xyloglucan endotransglucosylase/hydrolase involves in growth of primary root and alters the deposition of cellulose in *Arabidopsis*. *Planta*, 226, 1547–1560.
- Livingston, D. P. (1996). The second phase of cold hardening: Freezing tolerance and fructan isomer changes in winter cereal crowns. *Crop Science*, 36(6), 1568–1573.
- Livingston, D. P., & Henson, C. A. (1998). Apoplastic sugars, fructans, fructan exohydrolase, and invertase in winter oat: Responses to second-phase cold hardening. *Plant Physiology*, 116(1), 403–408.
- Livingston, D. P., Henson, C. A., Tuong, T. D., Wise, M. L., Tallury, S. P., & Duke, S. H. (2013). Histological analysis and 3D reconstruction of winter cereal crowns recovering from freezing: A unique response in oat (*Avena sativa* L.). *PLoS One*, 8(1), e53468.
- Livingston, D. P., & Tuong, T. D. (2014). Three-dimensional reconstruction of frozen and thawed plant tissues from microscopic images. In D. K. Hinch & E. Zuther (Eds.), *Methods in molecular biology* (Clifton, NJ) (Vol. 1166, pp. 117–137). New York, NY: USA Springer.
- Livingston, D. P., Tuong, T. D., Haigler, C. H., Avci, U., & Tallury, S. P. (2009). Rapid microwave processing of winter cereals for histology allows identification of separate zones of freezing injury in the crown. *Crop Science*, 49(5), 1837–1842.
- Livingston, D. P., Tuong, T. D., Hoffman, M., & Fernandez, G. (2018a). Protocol for producing three-dimensional infrared video of freezing in plants. *Journal of Visualized Experiments*, 139, e58025.
- Livingston, D. P., Tuong, T. D., Murphy, J. P., Gusta, L. V., Willick, I., & Wisniewski, M. E. (2018b). High-definition infrared thermography of ice nucleation and propagation in wheat under natural frost conditions and controlled freezing. *Planta*, 247(4), 791–806.
- Livingston, D. P., Van, K., Premakumar, R., Tallury, S. P., & Herman, E. M. (2007). Using *Arabidopsis thaliana* as a model to study subzero acclimation in small grains. *Cryobiology*, 54(2), 154–163.
- Marcus, S. E., Verhertbruggen, Y., Hervé, C., Ordaz-Ortiz, J. J., Farkas, V., Pedersen, H. L., ... Knox, J. P. (2008). Pectic homogalacturonan masks abundant sets of xyloglucan epitopes in plant cell walls. *BMC Plant Biology*, 8(1), 60.
- Maris, A., Kaewthai, N., Eklöf, J. M., Miller, J. G., Brumer, H., Fry, S. C., ... Vissenberg, K. (2011). Differences in enzymic properties of five recombinant xyloglucan endotransglucosylase/hydrolase (XTH) proteins of *Arabidopsis thaliana*. *Journal of Experimental Botany*, 62(1), 261–271.
- Miedes, E., Herbers, K., Sonnewald, U., & Lorences, E. P. (2010). Over-expression of a cell wall enzyme reduces xyloglucan depolymerization and softening of transgenic tomato fruits. *Journal of Agricultural and Food Chemistry*, 58(9), 5708–5713.
- Miedes, E., Suslov, D., Vandenbussche, F., Kenobi, K., Ivakov, A., Van Der Straeten, D., ... Vissenberg, K. (2013). Xyloglucan endotransglucosylase/hydrolase (XTH) overexpression affects growth and cell wall mechanics in etiolated *Arabidopsis hypocotyls*. *Journal of Experimental Botany*, 64(8), 2481–2497.
- Neumetzler, L. (2010). *Identification and characterization of Arabidopsis mutants associated with xyloglucan metabolism*. Berlin, Germany: Rhombos-Verlag.
- Neuner, G., Xu, B., & Hacker, J. (2010). Velocity and pattern of ice propagation and deep supercooling in woody stems of *Castanea sativa*, *Morus nigra* and *Quercus robur* measured by IDTA. *Tree Physiology*, 30(8), 1037–1045.
- Olien, C. R. (1984). An adaptive response of rye to freezing. *Crop Science*, 24(1), 51–54.
- Osato, Y., Yokoyama, R., & Nishitani, K. (2006). A principal role for AtXTH18 in *Arabidopsis thaliana* root growth: A functional analysis using RNAi plants. *Journal of Plant Research*, 119(2), 153–162.
- Panter, P. E., Kent, O., Dale, M., Smith, S. J., Skipsey, M., Thorlby, G., ... Knight, H. (2019). MUR1-mediated cell-wall fucosylation is required for freezing tolerance in *Arabidopsis thaliana*. *New Phytologist*, 224(4), 1518–1531.
- Park, Y. B., & Cosgrove, D. J. (2012). Changes in cell wall biomechanical properties in the xyloglucan-deficient xxt1/xtt2 mutant of *Arabidopsis*. *Plant Physiology*, 158(1), 465–475.
- Park, Y. B., & Cosgrove, D. J. (2015). Xyloglucan and its interactions with other components of the growing cell wall. *Plant and Cell Physiology*, 56(2), 180–194.
- Pauly, M., & Keegstra, K. (2016). Biosynthesis of the plant cell wall matrix polysaccharide xyloglucan. *Annual Review of Plant Biology*, 67(1), 235–259.
- Pearce, R. S. (1988). Extracellular ice and cell shape in frost-stressed cereal leaves: A low-temperature scanning-electron-microscopy study. *Planta*, 175(3), 313–324.
- Pearce, R. S., & Willison, J. H. M. (1985). Wheat tissues freeze-etched during exposure to extracellular freezing: distribution of ice. *Planta*, 163(3), 295–303.
- Pedersen, H. L., Fangel, J. U., McCleary, B., Ruzanski, C., Rydahl, M. G., Ralet, M.-C., ... Willats, W. G. T. (2012). Versatile high resolution oligosaccharide microarrays for plant glycobiology and cell wall research. *Journal of Biological Chemistry*, 287(47), 39429–39438.
- Pettolino, F. A., Walsh, C., Fincher, G. B., & Bacic, A. (2012). Determining the polysaccharide composition of plant cell walls. *Nature Protocols*, 7(9), 1590–1607.
- Pitaksaringkarn, W., Matsuoka, K., Asahina, M., Miura, K., Sage-Ono, K., Ono, M., ... Satoh, S. (2014). XTH20 and XTH19 regulated by ANAC071 under auxin flow are involved in cell proliferation in incised *Arabidopsis* inflorescence stems. *Plant Journal*, 80(4), 604–614.
- Rajashekar, C. B., & Burke, M. J. (1996). Freezing characteristics of rigid plant tissues (development of cell tension during extracellular freezing). *Plant Physiology*, 111(2), 597–603.
- Rajashekar, C. B., & Lafta, A. (1996). Cell wall changes and cell tension in response to cold acclimation and exogenous abscisic acid in leaves and cell cultures. *Plant Physiology*, 111(2), 605–612.
- Rose, J. K. C., Braam, J., Fry, S. C., & Nishitani, K. (2002). The XTH family of enzymes involved in xyloglucan endotransglucosylation and endohydrolysis: Current perspectives and a new unifying nomenclature. *Plant and Cell Physiology*, 43(12), 1421–1435.
- Shi, H., Ye, T., Zhong, B., Liu, X., Jin, R., & Chan, Z. (2014). AtHAP5A modulates freezing stress resistance in *Arabidopsis* through binding to CCAAT motif of AtXTH21. *New Phytologist*, 203, 554–567.
- Sims, I. M., Munro, S. L., Currie, G., Craik, D., & Bacic, A. (1996). Structural characterisation of xyloglucan secreted by suspension-cultured cells of *Nicotiana glauca*. *Carbohydrate Research*, 293(2), 147–172.

- Solecka, D., Zebrowski, J., & Kacperska, A. (2008). Are pectins involved in cold acclimation and de-acclimation of winter oil-seed rape plants? *Annals of Botany*, 101(4), 521–530.
- Stefanowska, M., Kuraś, M., Kubacka-Zębalska, M., & Kacperska, A. (1999). Low temperature affects pattern of leaf growth and structure of cell walls in winter oilseed rape (*Brassica napus* L., var. *Oleifera* L.). *Annals of Botany*, 84(3), 313–319.
- Steponkus, P. L. (1984). Role of the plasma membrane in freezing injury and cold acclimation. *Annual Review of Plant Physiology*, 35, 543–584.
- Takagi, T., Nakamura, M., Hayashi, H., Inatsugi, R., Yano, R., & Nishida, I. (2003). The leaf-order-dependent enhancement of freezing tolerance in cold-acclimated *Arabidopsis* rosettes is not correlated with the transcript levels of the cold-inducible transcription factors of CBF/DREB1. *Plant and Cell Physiology*, 44(9), 922–931.
- Takahashi, D., Gorka, M., Erban, A., Graf, A., Kopka, J., Zuther, E., & Hinch, D. K. (2019). Both cold and sub-zero acclimation induce cell wall modification and changes in the extracellular proteome in *Arabidopsis thaliana*. *Scientific Reports*, 9, 2289.
- Takahashi, D., Li, B., Nakayama, T., Kawamura, Y., & Uemura, M. (2013). Plant plasma membrane proteomics for improving cold tolerance. *Frontiers in Plant Science*, 4, 90.
- Takahashi, D., Zuther, E., & Hinch, D. K. (2020). Analysis of changes in plant cell wall and structure during cold acclimation. In D. K. Hinch & E. Zuther (Eds.), *Plant cold acclimation* (Vol. 2156, pp. 255–268). New York, NY: Springer US.
- Tenhaken, R. (2015). Cell wall remodeling under abiotic stress. *Frontiers in Plant Science*, 5, 771.
- Thalhammer, A., Hinch, D. K., & Zuther, E. (2014). Measuring freezing tolerance: Electrolyte leakage and chlorophyll fluorescence assays. In D. K. Hinch & E. Zuther (Eds.), *Plant cold acclimation* (Vol. 1166, pp. 15–24). New York, NY: Springer Science+Business Media.
- Thomashow, M. F. (2010). Molecular basis of plant cold acclimation: Insights gained from studying the CBF cold response pathway. *Plant Physiology*, 154(2), 571–577.
- Trunova, T. (1965). Light and temperature systems in the hardening of winter wheat and the significance of oligosaccharides for frost resistance. *Soviet Plant Physiology*, 12, 70–77.
- Uemura, M., Joseph, R. A., & Steponkus, P. L. (1995). Cold acclimation of *Arabidopsis thaliana* (effect on plasma membrane lipid composition and freeze-induced lesions). *Plant Physiology*, 109(1), 15–30.
- Updegraff, D. M. (1969). Semimicro determination of cellulose in biological materials. *Analytical Biochemistry*, 32(3), 420–424.
- Valluru, R., Lammens, W., Claupein, W., & Van den Ende, W. (2008). Freezing tolerance by vesicle-mediated fructan transport. *Trends in Plant Science*, 13(8), 409–414.
- Valluru, R., & Van den Ende, W. (2008). Plant fructans in stress environments: Emerging concepts and future prospects. *Journal of Experimental Botany*, 59(11), 2905–2916.
- Vissenberg, K., Oyama, M., Osato, Y., Yokoyama, R., Verbelen, J.-P., & Nishitani, K. (2005). Differential expression of AtXTH17, AtXTH18, AtXTH19 and AtXTH20 genes in *Arabidopsis* roots. Physiological roles in specification in cell wall construction. *Plant and Cell Physiology*, 46(1), 192–200.
- Voxeur, A., & Höfte, H. (2016). Cell wall integrity signaling in plants: “To grow or not to grow that's the question”. *Glycobiology*, 26(9), 950–960.
- Weiser, R. L., Wallner, S. J., & Waddell, J. W. (1990). Cell wall and extensin mRNA changes during cold acclimation of pea seedlings. *Plant Physiology*, 93(3), 1021–1026.
- Willick, I. R., Takahashi, D., Fowler, D. B., Uemura, M., & Tanino, K. K. (2018). Tissue-specific changes in apoplastic proteins and cell wall structure during cold acclimation of winter wheat crowns. *Journal of Experimental Botany*, 69(5), 1221–1234.
- Wilson, M. H., Holman, T. J., Sørensen, I., Cancho-Sanchez, E., Wells, D. M., Swarup, R., ... Hodgman, T. C. (2015). Multi-omics analysis identifies genes mediating the extension of cell walls in the *Arabidopsis thaliana* root elongation zone. *Frontiers in Cell and Developmental Biology*, 3, 10.
- Wisniewski, M., Lindow, S. E., & Ashworth, E. N. (1997). Observations of ice nucleation and propagation in plants using infrared video thermography. *Plant Physiology*, 113(2), 327–334.
- Zhang, T., Tang, H., Vavylonis, D., & Cosgrove, D. J. (2019). Disentangling loosening from softening: Insights into primary cell wall structure. *Plant Journal*, 100(6), 1101–1117.
- Zhu, X. F., Shi, Y. Z., Lei, G. J., Fry, S. C., Zhang, B. C., Zhou, Y. H., ... Zheng, S. J. (2012). XTH31, encoding an in vitro XEH/XET-active enzyme, regulates aluminum sensitivity by modulating in vivo XET action, cell wall xyloglucan content, and aluminum binding capacity in *Arabidopsis*. *Plant Cell*, 24(11), 4731–4747.
- Zuther, E., Schaarschmidt, S., Fischer, A., Erban, A., Pagter, M., Mubeen, U., ... Hinch, D. K. (2019). Molecular signatures associated with increased freezing tolerance due to low temperature memory in *Arabidopsis*. *Plant, Cell & Environment*, 42(3), 854–873.
- Zuther, E., Schulz, E., Childs, L. H., & Hinch, D. K. (2012). Clinal variation in the non-acclimated and cold-acclimated freezing tolerance of *Arabidopsis thaliana* accessions. *Plant, Cell & Environment*, 35(10), 1860–1878.

SUPPORTING INFORMATION

Additional supporting information may be found online in the Supporting Information section at the end of this article.

How to cite this article: Takahashi D, Johnson KL, Hao P, et al. Cell wall modification by the xyloglucan endotransglucosylase/hydrolase XTH19 influences freezing tolerance after cold and sub-zero acclimation. *Plant Cell Environ*. 2021;44:915–930. <https://doi.org/10.1111/pce.13953>